Experimental Verification of Morphological Instability in Freezing Aqueous Colloidal Suspensions

S. S. L. Peppin[1] and J. S. Wettlaufer[1,2]

[1]*Department of Geology and Geophysics, Yale University, New Haven, Connecticut 06520, USA*
[2]*Department of Physics, Yale University, New Haven, Connecticut 06520, USA*

M. G. Worster

Institute of Theoretical Geophysics, Department of Applied Mathematics and Theoretical Physics, Cambridge University,
Cambridge CB3 0WA, United Kingdom

We describe an experimental test of a new theory of the unidirectional freezing of aqueous colloidal suspensions. At low freezing speeds a planar ice lens completely rejects the particles, forming a steady-state compacted boundary layer in the liquid region. At higher speeds the planar interface becomes thermodynamically unstable and breaks down geometrically to trap bulk regions of colloid within. The theoretical stability threshold is determined experimentally, thereby demonstrating that colloidal suspensions can be treated analogously to atomic or molecular alloys.

PACS numbers: 82.70.Dd, 64.75.Xc

Structure formation during crystal growth is an important example of self-organization in systems driven away from equilibrium [1]. Owing to their intrinsic complexity and technological importance, pure materials and molecular solutions have been the focus of intense theoretical and experimental studies over the past several decades [2]. Recently attention has been paid to colloidal systems [3–6], which also display a fascinating variety of patterns upon freezing (Fig. 1). Besides presenting new challenges to our understanding of colloidal physics, the self-organization of freezing colloids plays an important role in many natural and technological processes. The phenomenon underlies frost heave and patterned ground [7,8], influences the success of cryopreservation [9], and provides a mechanism for the remediation of contaminated clay [10,11]. At low initial particle concentrations it is possible to remove the segregated ice by freeze drying to yield microaligned porous materials with uses in bioengineering and microfluidics [4,12]. Despite the large number of applications, many questions remain about the fundamental mechanisms underlying the solidification of colloidal systems.

In liquid solutions the phenomenon of constitutional supercooling, in which the temperature of the melt directly in front of the freezing interface is below its equilibrium freezing temperature, governs the onset of morphological instability [2,13]. Although it is known experimentally that colloidal particles can profoundly affect the nature of the instability [14], it has not been clear how best to account for colloidal effects, especially if the particle concentration is high. Most theoretical and experimental studies have therefore focused on the interaction between an isolated colloidal particle and the solid–liquid interface [15,16].

Recently, it has been recognized that in concentrated systems the colloidal suspension itself can become constitutionally supercooled [5,17]. A theoretical framework describing this phenomenon has been developed by taking into account the strong concentration dependence of the governing parameters in colloidal systems (diffusivity, osmotic pressure, etc.) [5,6]. Theory predicts that even in the absence of ionic solutes the freezing interface can become morphologically unstable owing to the effects of the colloidal particles alone. In the present work we test this theory on colloidal bentonite. We first discuss the overall geometry of the experiment, the equilibrium phase diagram, and dynamic properties of the colloid. Measurements of the compressibility (osmotic pressure) are used to predict the freezing point depression as a function of particle volume fraction. Finally, measurements of the permeability are employed to predict the concentration-dependent diffusivity. These properties enable us to construct a quantitative model of the solidification process, and to determine conditions under which constitutional supercooling occurs.

We consider a system in which a layer of colloid at initial volume fraction ϕ_0 is placed to height L_0 in a water-filled glass cell between two fixed temperature
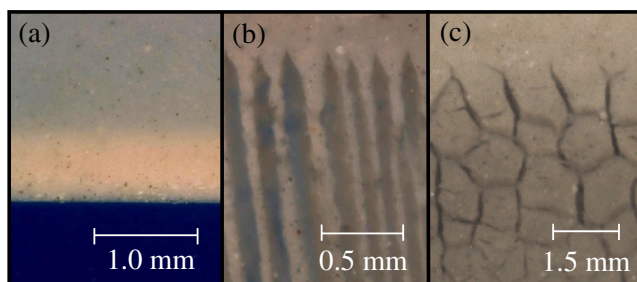

FIG. 1 (color online). Segregated ice (darker regions) formed during the unidirectional solidification of a colloidal suspension (bentonite). Depending on the particle concentration, temperature gradient, and freezing rate, the ice (a) rejects the particles, (b) forms aligned dendrites, or (c) forms polygons.

blocks (Fig. 2). A temperature gradient G_T is maintained by holding the blocks at temperatures T_H and T_C with $T_H > T_f(\phi_0) > T_C$, where $T_f(\phi_0)$ is the freezing temperature of the bulk suspension. The cell is moved through the blocks at a fixed speed V. We consider speeds $V \ll V_c$, where V_c is the critical engulfment speed of an individual colloidal particle. (For submicron hydrophilic particles $V_c > 10$ μm s^{-1} [15,18].) All of the particles will therefore be pushed ahead by the growing ice and, if the interface remains stable, a continuous layer of ice will grow at steady state, pushing ahead a consolidated colloid boundary layer.

In order to obtain the concentration-dependent freezing temperature, we consider a system in which a portion of ice is in equilibrium with a quantity of unfrozen colloid [19]. As the temperature is lowered, the ice phase grows and the water content of the colloid decreases. The freezing temperature can be obtained by equating the chemical potential of water in the unfrozen colloid with the chemical potential of pure ice [5,20]. For temperatures near to the freezing temperature of pure water T_m, this leads to the relation

$$T_f(\phi) = T_m \left[1 - \frac{\Pi(\phi)}{\rho_\ell L_f} \right], \qquad (1)$$

where ρ_ℓ and L_f are the density and latent heat of fusion, respectively, of water. In order to use Eq. (1), knowledge of the osmotic pressure $\Pi(\phi)$ is required. Figure 3(a) shows measurements of $\Pi(\phi)$ obtained from several sources. To fit the data over the full range in ϕ we use a virial-type expression in the form

$$\frac{v_p \Pi(\phi)}{k_B T_m} = \phi \frac{1 + \Sigma b_k \phi^k}{1 - \phi/\phi_p}, \qquad (2)$$

where $v_p = \frac{4}{3}\pi R^3$ is the volume of a bentonite particle of

hydrodynamic radius $R = 0.5$ μm [21] and k_B is Boltzmann's constant. The empirical coefficients b_k account for long range electrostatic, structural, and van der Waals interactions between the colloidal particles, while the $1 - \phi/\phi_p$ factor allows for excluded volume effects near the shrinkage limit. The solid curve in Fig. 3(a) shows the fit to the data, and the resulting prediction for $T_f(\phi)$ is compared with experimental measurements in Fig. 3(b). The agreement is excellent for temperatures near or above -5 °C, which are relevant to our analysis. The dashed line in Fig. 3(b) is a reminder that pore ice may exist below -8 °C [19], in which case alternative methods can be used to predict the liquid fraction as a function of temperature [22,23].

Figure 4 shows measurements of the permeability of bentonite. The solid curve is a fit of the data in the form $k(\phi) = k_0[1 + (3.1 \times 10^8)\phi^{2.6}]^{-1}$ where $k_0 = 2R^2/9\phi$. As shown previously [5], in colloidal suspensions one is free to choose either Darcy's law or Fick's law to describe the colloid mass flux. The two equations are related by a generalized form of the Stokes-Einstein relation

$$D(\phi) = \phi \frac{k(\phi)}{\mu} \left(\frac{\partial \Pi}{\partial \phi} \right)_{T,P}, \qquad (3)$$

where D is the particle diffusivity, μ is the dynamic viscosity of the fluid, T is the absolute temperature, and P is the mixture pressure. Given measurements of the permeability and osmotic pressure, Eq. (3) determines the diffusivity as a function of volume fraction.

A typical experiment with freezing velocity $V = 0.1$ μm s^{-1} is shown in Fig. 5. In Fig. 5(a) we observe the consolidation of the boundary layer above the ice-colloid interface as the system approaches steady state.
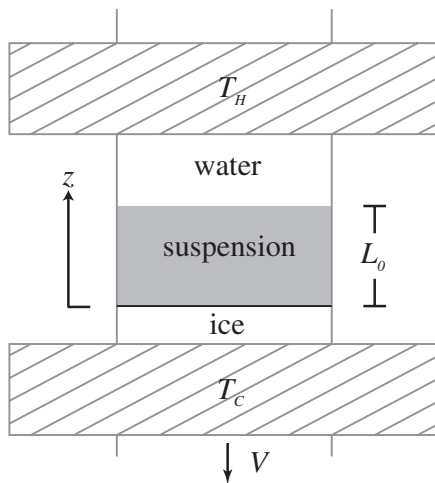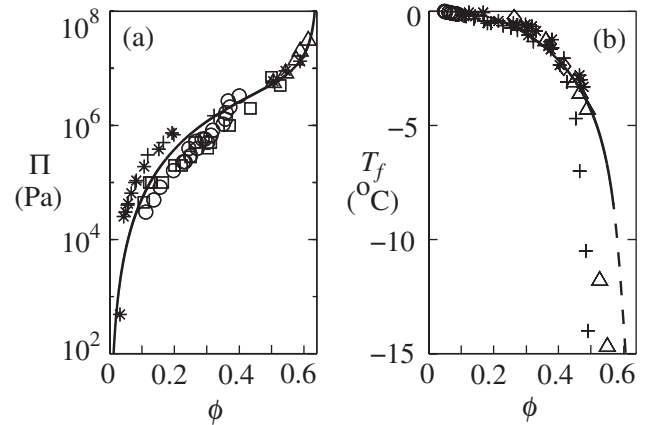

FIG. 2. Schematic of the unidirectional solidification stage. The height, width, and depth of the cell between the blocks are 6 cm, 12 cm, and 0.5 cm, respectively. A detailed description of the experimental apparatus is given in Ref. [25].

FIG. 3. (a) Measurements of the osmotic pressure of bentonite as a function of particle volume fraction ($\triangle$ [20]; $*$ [26]; $\square$ [27]; $\bigcirc$ [28]). The solid curve is a fit of the data to Eq. (2) using $b_3 = 8 \times 10^9$, $b_4 = -2 \times 10^{10}$, $b_5 = 1.3 \times 10^{10}$, and $\phi_p = 0.64$. (b) Prediction from Eq. (1) (solid curve) and measurements (symbols) of the freezing point depression of bentonite ($\triangle$ [29]; $+$ [19]; $\bigcirc$ [30]; $*$ [31]).
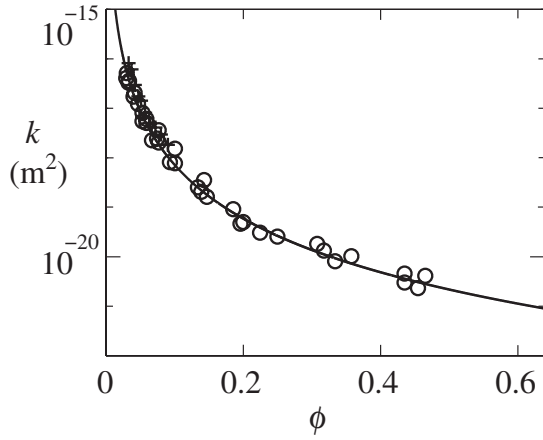
FIG. 4. Measurements of the permeability of bentonite as a function of particle volume fraction ($\bigcirc$, Mesri and Olson [32]; +, Kirby and Smiles [33]). The solid curve is a fit of the data.

In Fig. 5(b) the colloidal suspension has fully consolidated to a steady-state thickness of 3 mm. When the freezing velocity is increased to 0.8 μm s^{-1} [Fig. 5(c)], the planar interface destabilizes, leading to the formation of segregated ice in the interior of the layer [Fig. 5(d)].

In order to uncover the essential governing parameters, it is useful to model the system by scaling lengths with $\phi_0 L_0$ and temperatures with T_m. In a frame of reference moving at the freezing speed V, the steady-state concentration profile is then determined by the equation

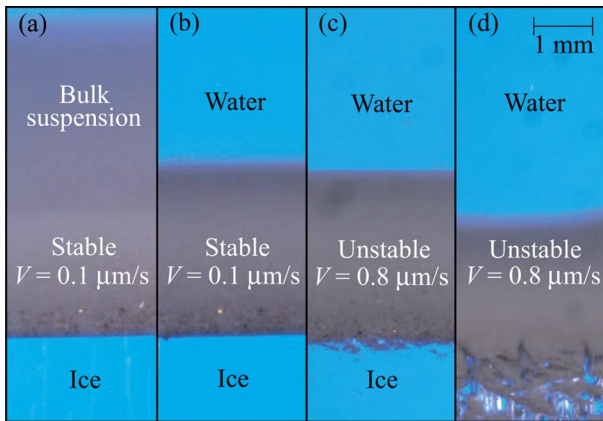$$\frac{d\phi}{d\hat{z}} = -\mathrm{Pe}\,\frac{\phi}{\hat{D}(\phi)}, \tag{4}$$

where $\hat{z} = z/\phi_0 L_0$, $\mathrm{Pe} = V\phi_0 L_0/D_0$ is the Peclet number, $\hat{D} = D/D_0$ is the dimensionless diffusivity, and $D_0 = k_B T_m/6\pi R\mu$ is the Stokes-Einstein diffusivity of an isolated colloidal particle. A boundary condition for (4) at $\hat{z} = 0$ can be obtained by using global mass conservation in the form

$$\mathrm{Pe} = \int_0^{\phi_i} \hat{D}(\phi)d\phi, \tag{5}$$

where ϕ_i is the volume fraction at the ice-colloid interface.

Once the concentration profile is determined from (4) and (5), the freezing temperature profile can be obtained from (1). For a linear temperature gradient the steady-state temperature profile in the colloid is given by

$$\hat{T}(\hat{z}) = \hat{T}_f(\phi_i) + \mathcal{G}_T\hat{z}, \tag{6}$$

where $\hat{T}_f(\phi_i) = T_f(\phi_i)/T_m$ is the dimensionless temperature at the ice-colloid interface and $\mathcal{G}_T = G_T L_0\phi_0/T_m$ is the dimensionless temperature gradient.

For a given temperature gradient, the critical conditions for the onset of constitutional supercooling can be obtained from the equation

$$\mathcal{G}_T \leq \left.\frac{d\hat{T}_f}{d\hat{z}}\right|_{\hat{z}=0} = -\mathrm{Pe}\hat{T}_{f\phi}\frac{\phi_i}{\hat{D}}, \tag{7}$$

where $\hat{T}_{f\phi} = d\hat{T}_f/d\phi$ and ϕ_i is determined as a function of Pe from Eq. (5). In our experiments ϕ_0 and G_T were kept constant while only L_0 and V were varied. The curve $L_0(V)$ obtained from (7) with no adjustable parameters is shown on Fig. 6, along with experimental data. To the right of the curve the colloid is predicted to be constitutionally

FIG. 5 (color online). Unidirectional solidification of colloidal bentonite ($\phi_0 = 0.02$, $L_0 = 7$ mm, and $G_T = 5\,°C/cm$). (a) The partially consolidated colloid boundary layer, which formed above a planar ice interface during an experiment at $V = 0.1\,\mu$m s^{-1}. Eventually the colloid fully consolidated and the system reached steady state (b). In (c) the freezing speed was increased to 0.8 μm s^{-1} and the ice−colloid interface became unstable, with segregated ice eventually forming in the colloid interior (d).
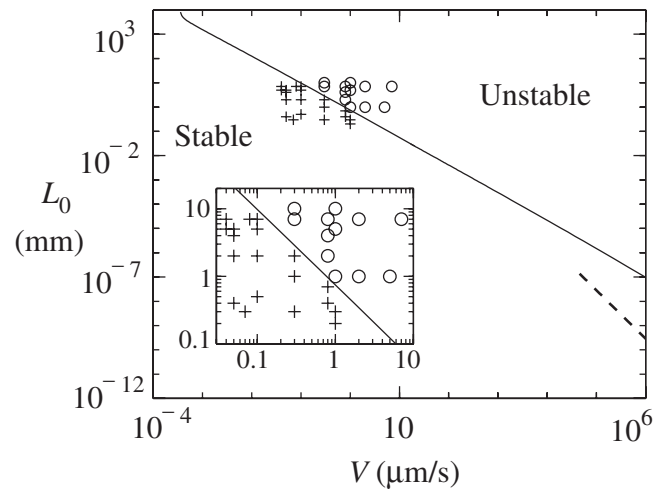

FIG. 6. Regime diagram for the steady-state solidification of colloidal bentonite. The solid and dashed curves are from Eq. (7) using the concentration-dependent and dilute expressions, respectively, for the governing parameters. The crosses and circles represent experiments where the freezing interface was stable and unstable, respectively. The inset shows a close-up view of the data.

supercooled. The open circles represent experiments where the interface became nonplanar and the crosses represent experiments where the ice interface remained planar at steady state.

The data confirm our treatment of the colloidal suspension using the appropriately modified criterion for constitutional supercooling that drives a morphological instability of the freezing interface. One important aspect distinguishing morphological instability in colloidal systems from alloys and aqueous solutions is the strongly nonlinear concentration dependence of the transport properties. To illustrate this effect, in Fig. 6 we show the prediction obtained by using the dilute value for the diffusivity, D_0, and the dilute freezing temperature slope $\Gamma_0 = -(k_B T_m^2)/(\rho_\ell L_f v_p)$. Extending the dashed curve any closer to the data leads to the unphysical prediction $\phi_i > 1$. The very poor agreement in this case illustrates the novel distinction between this system and most atomic or molecular alloys; in colloidal suspensions we must properly account for the concentration dependence of the relevant governing parameters.

Our directional solidification experiments provide a test bed for the theory of morphological stability in colloidal suspensions. Thus the phenomenon of constitutional supercooling, originally developed to describe such instabilities in atomic metals [13], has a novel manifestation in this ''colloidal alloy'' wherein we must account for both the consolidation of the colloid through a concentration-dependent diffusivity and a nonlinear freezing temperature curve. We quantitatively characterize the morphological instability of a single ice layer as the abrupt transition to segregated freezing wherein the bulk colloid is trapped within the ice phase. The results and analysis provide an essential step toward quantifying the morphological transitions observed in freezing colloidal suspensions [4,12]. In addition, we have experimentally confirmed a new mechanism for the formation of segregated ice in colloidal clays, which may help to explain experimental and field observations of unfrozen clay and silt between ice lenses [19,24]. Perhaps of wider interest is the fact that an easily accessible steady state has been achieved prior to instability. This suggests the intriguing possibility of exploiting colloids to study the onset and growth of morphological instabilities in molecular systems and in other systems yet to be explored.

[1] M. C. Cross and P. C. Hohenberg, Rev. Mod. Phys. **65**, 851 (1993).

[2] S. H. Davis, *Theory of Solidification* (Cambridge University Press, U.K., 2001).

[3] K. Watanabe and M. Mizoguchi, J. Cryst. Growth **213**, 135 (2000).

[4] S. Deville, E. Saiz, R. K. Nalla, and A. P. Tomsia, Science **311**, 515 (2006).

[5] S. S. L. Peppin, J. A. W. Elliot, and M. G. Worster, J. Fluid Mech. **554**, 147 (2006).

[6] S. S. L. Peppin, M. G. Worster, and J. S. Wettlaufer, Proc. R. Soc. A **463**, 723 (2007).

[7] S. Taber, J. Geol. **37**, 428 (1929).

[8] B. Hallet, Can. J. Phys. **68**, 842 (1990).

[9] P. Mazur, Science **168**, 939 (1970).

[10] R. Dawson, D. Sego, and G. Pollock, Can. Geotech. J. **36**, 587 (1999).

[11] G. Gayand and A. M. Azouni, Cryst. Growth Des. **2**, 135 (2002).

[12] H. Zhang and A. I. Cooper, Adv. Mater. **19**, 1529 (2007).

[13] W. W. Mullins and R. F. Sekerka, J. Appl. Phys. **35**, 444 (1964).

[14] J. A. Sekhar and R. Trivedi, Mater. Sci. Eng. A **147**, 9 (1991).

[15] D. R. Uhlmann, B. Chalmers, and K. A. Jackson, J. Appl. Phys. **35**, 2986 (1964).

[16] A. W. Rempel and M. G. Worster, J. Cryst. Growth **205**, 427 (1999).

[17] M. F. Butler, Cryst. Growth Des. **1**, 213 (2001).

[18] J. Cisse and G. F. Bolling, J. Cryst. Growth **10**, 67 (1971).

[19] S. C. Brown and D. Payne, J. Soil Sci. **41**, 547 (1990).

[20] P. F. Low, D. M. Anderson, and P. Hoekstra, Water Resour. Res. **4**, 379 (1968).

[21] B. E. Novich and T. A. Ring, Clays Clay Miner. **32**, 400 (1984).

[22] J. W. Cahn, J. G. Dash, and H.-Y. Fu, J. Cryst. Growth **123**, 101 (1992).

[23] J. G. Dash, A. W. Rempel, and J. S. Wettlaufer, Rev. Mod. Phys. **78**, 695 (2006).

[24] G. Beskow, The Swedish Geological Society, C, no. 375, Year Book no. 3 (Technological Institute, Northwestern University, 1935), reprinted in Historical Perspectives in Frost Heave Research (P. B. Black and M. J. Hardenberg, eds.), CRREL Special Report No. 91-23, p. 37, 1991.

[25] S. S. L. Peppin, P. Aussillous, H. E. Huppert, and M. G. Worster, J. Fluid Mech. **570**, 69 (2007).

[26] J. L. Oliphant and P. F. Low, J. Colloid Interface Sci. **89**, 366 (1982).

[27] J. D. Sherwood, G. H. Meeten, C. A. Farrow, and N. J. Alderman, J. Chem. Soc., Faraday Trans. **87**, 611 (1991).

[28] J. D. Sherwood and G. H. Meeten, J. Pet. Sci. Eng. **18**, 73 (1997).

[29] D. M. Anderson, Isr. J. Chem. **6**, 349 (1968).

[30] R. W. R. Koopmans and R. D. Miller, Soil Sci. Soc. Am. J. **30**, 680 (1966).

[31] T. Kozlowski, Cold Reg. Sci. Technol. **38**, 93 (2004).

[32] G. Mesri and R. E. Olson, Geotechnique **21**, 341 (1971).

[33] J. M. Kirby and D. E. Smiles, Aust. J. Soil Res. **26**, 561 (1988).